

Quantum theory of superresolution for two incoherent optical point sources

Mankei Tsang,^{1,2,*} Ranjith Nair,¹ and Xiaoming Lu¹

¹*Department of Electrical and Computer Engineering,
National University of Singapore, 4 Engineering Drive 3, Singapore 117583*

²*Department of Physics, National University of Singapore, 2 Science Drive 3, Singapore 117551*

(Dated: May 5, 2022)

We prove that Rayleigh’s criterion is fundamentally irrelevant to the localization of two incoherent point sources in far-field optical imaging. This is done in two ways: (1) We derive the quantum Cramér-Rao error bound for the problem under standard assumptions for thermal optical sources, and the bound shows little sign of the accuracy degradation that plagues conventional imaging when Rayleigh’s criterion is violated. (2) We propose a linear optical measurement method called spatial-mode demultiplexing (SPADE) that can attain the quantum bound for separation estimation regardless of the distance between the sources, a task conventional methods perform poorly for close sources. These results demonstrate that Rayleigh’s criterion is nothing but a technicality specific to conventional imaging, and cleverer quantum measurements can locate two incoherent sources with arbitrary separation almost as accurately as conventional methods do for isolated sources.

I. INTRODUCTION

How well can an optical instrument see? No question is more important in optics, and pushing the limits of optical imaging resolution to distinguish smaller or farther objects is not only an obsession of optics researchers but also of practical importance to nanoscience, biology, remote sensing, and astronomy. Rayleigh’s criterion for resolving two incoherent point sources [1, 2] has been the most influential measure of optical resolution for over a century, but insights from quantum optics [3] and statistics [4] have since led to revolutions in far-field superresolution techniques [5–7] beyond his criterion. The techniques proposed in Refs. [3, 4] rely on accurately locating a point source when no other nearby sources are radiating. While such techniques have achieved spectacular success, they place stringent conditions on the sources to ensure that close sources are not radiating at the same time.

To overcome this restriction, an important work by Ram, Ward, and Ober [8] points out that, when two point sources are close and both radiating, statistical estimation using the data of image-plane photon counting can still determine their locations, although the accuracy for a given photon number quickly deteriorates when the separation between the point sources becomes smaller than the width of the imaging point-spread function. The accuracy degradation is mandated by the Cramér-Rao bound [9, 10], which sets a lower bound on the estimation error for any (unbiased) estimator, suggesting that the degradation is fundamental to the image-plane photon-counting method. Given the prior work up to this point, conventional wisdom thus suggests that the positions of two point sources should become harder to estimate when their radiations overlap, a phenomenon we call *Rayleigh’s curse*.

Our recent work [11], on the other hand, has given us fresh impetus to attack the resolution problem from the alternative perspective of quantum metrology [12–14], which is a branch of quantum information theory relevant to sensing and imaging. Instead of limiting our imagination by studying existing imaging techniques, the central theme of quantum metrology is to seek the general mathematical and physical forms of measurements that can achieve fundamental limits to statistical inference set by the laws of quantum mechanics. While our previous work focuses on coherent sources with only passing comments on incoherent sources, here we embark on the derivation of the fundamental quantum limit to the localization of two incoherent thermal optical point sources in the form of the quantum Cramér-Rao bound (QCRB) [12–14]. Surprisingly, we find that the QCRB maintains a fairly constant value for any separation and shows no serious accuracy degradation when the two sources are close.

The asymptotic attainability of the QCRB for single-parameter estimation has been proved in a seminal work by Fujiwara [15], meaning that there formally exists a quantum measurement scheme that has an error asymptotically attaining the QCRB over many trials. This attainability motivates us to find a more realistic imaging method that can approach the bound, and here we propose such a method called spatial-mode demultiplexing (SPADE). Spatial mode-division multiplexing and demultiplexing is a coherent optical technique of current experimental interest in quantum optics [16, 17] as well as optical communication [18]. We show that SPADE can ideally estimate the separation between the two sources with a classical Fisher information equal to the quantum value, and we also propose linear optical system designs that can implement the measurement. Image-plane photon counting is inaccurate for two close point sources precisely because it estimates their separation poorly, and SPADE is able to overcome this problem and Rayleigh’s curse via further coherent linear optical processing before photon counting.

* mankei@nus.edu.sg

The subject of quantum imaging has been extensively researched (see, for example, Refs. [12, 19–35]), but most prior proposals rely on nonclassical sources and/or multiphoton coincidence measurements, making them difficult and inefficient to use in practice. Incoherent sources such as stars and fluorescent markers are of course much more common, and linear optical methods to enhance the localization accuracy for close incoherent sources will be of monumental interest to both telescopes and microscopes. The most relevant prior work remains the pioneering studies by Helstrom on thermal sources [12], yet he studied two sources only in the context of binary hypothesis testing and assumed a given separation in the two-source hypothesis [36]. As the separation is usually unknown and needs to be estimated in the first place, our framework should be more useful.

II. QUANTUM OPTICS

A. Thermal optical state

To illustrate the essential physics, we follow Lord Rayleigh's lead [1] and assume quasi-monochromatic paraxial waves with one polarization and one spatial dimension on the object and image planes. Consider an optical imaging system, such as a microscope or a telescope, and divide the image plane into many pixels. The measurement on each pixel can be conceptualized as a measurement on the optical wavepacket mode specific to that pixel [19]. Denote a multimode coherent state as $|\alpha\rangle$, where $\alpha \equiv (\alpha_1, \alpha_2, \dots, \alpha_J)$ is a vector of complex amplitudes for the wavepacket modes. The quantum density operator characterizing an arbitrary optical field on the image plane within the coherence time can then be expressed as

$$\rho = \int D\alpha \Phi(\alpha) |\alpha\rangle \langle \alpha|, \quad (2.1)$$

where $\Phi(\alpha)$ is the Sudarshan-Glauber representation, $D\alpha \equiv d^2\alpha_1 d^2\alpha_2 \dots d^2\alpha_J$, and $d^2\alpha_j \equiv d(\text{Re } \alpha_j) d(\text{Im } \alpha_j)$ [37].

To model a thermal source at an optical frequency or beyond, it is reasonable and standard [37, 38] to assume that, within the short coherence time of the source, the probability that a photon arrives at the imaging device is small, and useful information is acquired only after many photons have been collected. We will make the same assumption for two sources, and assume the following low-dimensional approximation of the coherent state:

$$|\alpha\rangle \approx \sqrt{\pi_0} |\text{vac}\rangle + \sum_j \alpha_j |j\rangle, \quad |j\rangle \equiv a_j^\dagger |\text{vac}\rangle, \quad (2.2)$$

where $|\text{vac}\rangle$ denotes the vacuum state, $\pi_0 = 1 - \sum_j |\alpha_j|^2$, $|j\rangle$ denotes the state with one photon only in the j th mode, satisfying the orthogonality conditions

$$\langle \text{vac} | j \rangle = 0, \quad \langle j | k \rangle = \delta_{jk}, \quad (2.3)$$

and a_j^\dagger is the creation operator for the j th mode. The low-dimensional approximation leads to

$$\begin{aligned} \rho \approx & (1 - \epsilon) |\text{vac}\rangle \langle \text{vac}| + \sum_{j,k} \mathbb{E}(\alpha_j \alpha_k^*) |j\rangle \langle k| \\ & + \sum_j [\mathbb{E}(\alpha_j) |j\rangle \langle \text{vac}| + \mathbb{E}(\alpha_j^*) |\text{vac}\rangle \langle j|], \end{aligned} \quad (2.4)$$

where

$$\epsilon = \sum_j \mathbb{E}(|\alpha_j|^2) \ll 1 \quad (2.5)$$

is the small probability of having one photon in all modes, and

$$\mathbb{E}[f(\alpha)] \equiv \int D\alpha \Phi(\alpha) f(\alpha) \quad (2.6)$$

is the expectation of any function of α with respect to the Φ distribution. For sources with random phases, the mean field $\mathbb{E}(\alpha_j)$ vanishes, and we are left with

$$\rho \approx (1 - \epsilon) |\text{vac}\rangle \langle \text{vac}| + \sum_{j,k} \mathbb{E}(\alpha_j \alpha_k^*) |j\rangle \langle k|. \quad (2.7)$$

A similar framework was used in Ref. [39] to study stellar interferometry. We will hereafter restrict our attention to the zero/one-photon sector; multiphoton events for a thermal source have a probability $O(\epsilon^2)$, happen much more rarely at optical frequencies as $\epsilon \ll 1$, and can contribute relatively little information. This restriction also makes our model applicable to incoherent and inefficient single-photon emitters, which may have nonclassical multiphoton statistics but relatively few multiphoton events.

$\mathbb{E}(\alpha_j \alpha_k^*)$ is the mutual coherence [37], determined by the mutual coherence on the object plane as well as the field propagation in the imaging system. Let β_u be the field amplitude on the object plane, with u indexing the spatial modes there. For a linear optical system, the propagation of coherent states is governed by the rule

$$\alpha_j = \sum_u F_{ju} \beta_u, \quad (2.8)$$

where F_{ju} is the impulse-response matrix [40]. Then the image-plane coherence is determined by

$$\mathbb{E}(\alpha_j \alpha_k^*) = \sum_{u,v} F_{ju} \mathbb{E}_b(\beta_u \beta_v^*) F_{kv}^*. \quad (2.9)$$

where \mathbb{E}_b is the expectation with respect to the object-plane Sudarshan-Glauber representation. This propagation rule is a basic principle in both classical and quantum statistical optics [37].

B. Two incoherent sources

Consider two incoherent sources with equal intensities at positions $u = u_1$ and $u = u_2$. The fields are uncorrelated at different points on the object plane, with nonzero

intensities only at the sources, viz.,

$$\mathbb{E}_b(\beta_u \beta_v^*) = \epsilon_0 \delta_{uv} (\delta_{uu_1} + \delta_{uu_2}), \quad (2.10)$$

where ϵ_0 is the average photon number from each source. This results in an image-plane coherence given by

$$\mathbb{E}(\alpha_j \alpha_k^*) = \epsilon_0 F_{ju_1} F_{ku_1}^* + \epsilon_0 F_{ju_2} F_{ku_2}^*. \quad (2.11)$$

The one-photon probability becomes

$$\epsilon = 2\epsilon_0 \eta, \quad (2.12)$$

where

$$\eta \equiv \sum_j |F_{ju_1}|^2 = \sum_j |F_{ju_2}|^2 \quad (2.13)$$

is the quantum efficiency of the imaging system and we have made the reasonable assumption that the efficiency is the same for both sources. Defining the following single-photon states:

$$|\psi_1\rangle \equiv \sum_j \psi_{ju_1} |j\rangle, \quad \psi_{ju_1} \equiv \frac{1}{\sqrt{\eta}} F_{ju_1}, \quad (2.14)$$

$$|\psi_2\rangle \equiv \sum_j \psi_{ju_2} |j\rangle, \quad \psi_{ju_2} \equiv \frac{1}{\sqrt{\eta}} F_{ju_2}, \quad (2.15)$$

with ψ_{ju_1} and ψ_{ju_2} being the normalized wavefunctions ($\langle\psi_1|\psi_1\rangle = \sum_j |\psi_{ju_1}|^2 = \langle\psi_2|\psi_2\rangle = \sum_j |\psi_{ju_2}|^2 = 1$), we can rewrite the density operator in Eq. (2.7) as

$$\rho = (1 - \epsilon) |\text{vac}\rangle \langle\text{vac}| + \frac{\epsilon}{2} (|\psi_1\rangle \langle\psi_1| + |\psi_2\rangle \langle\psi_2|). \quad (2.16)$$

This is the central form of the quantum optical state that we will use for the rest of the paper.

C. Image-plane photon counting

We can recover the semiclassical model of image-plane photon counting [8, 38] by considering the photon statistics of Eq. (2.16). With at most one photon in the assumed state, we only need to consider the probability of no photon given by

$$\langle\text{vac}|\rho|\text{vac}\rangle = 1 - \epsilon, \quad (2.17)$$

and the probability of finding one photon at the j th pixel on the image plane given by

$$\langle j|\rho|j\rangle = \frac{\epsilon}{2} (|\psi_{ju_1}|^2 + |\psi_{ju_2}|^2). \quad (2.18)$$

With our $\epsilon \ll 1$ assumption, these can be approximated as the Poissonian distribution

$$P(n_1, n_2, \dots, n_J) = \prod_j \exp(-\epsilon \Lambda_j) \frac{(\epsilon \Lambda_j)^{n_j}}{n_j!}, \quad (2.19)$$

$$\Lambda_j = \frac{1}{2} (|\psi_{ju_1}|^2 + |\psi_{ju_2}|^2), \quad (2.20)$$

as

$$P(0, \dots) \approx 1 - \epsilon = \langle\text{vac}|\rho|\text{vac}\rangle, \quad (2.21)$$

$$P(0, \dots, n_j = 1, 0, \dots) \approx \epsilon \Lambda_j = \langle j|\rho|j\rangle, \quad (2.22)$$

and multiphoton probabilities are negligible. With Poissonian statistics for one trial, the total count at each pixel over M trials also becomes Poissonian, with a distribution

$$P^{(M)}(n_1, n_2, \dots, n_J) \approx \prod_j \exp(-N \Lambda_j) \frac{(N \Lambda_j)^{n_j}}{n_j!}, \quad (2.23)$$

where

$$N \equiv M \epsilon = 2M \epsilon_0 \eta \quad (2.24)$$

is the average photon number from both sources collected over the M trials. Eq. (2.23) is precisely the standard shot-noise model for thermal sources at optical frequencies in semiclassical statistical optics [38] and also used by Ram *et al.* [8]. The mean photon count is $N \Lambda_j$, which is determined by the incoherent sum of the wavefunctions in Eq. (2.20), as expected from semiclassical arguments [38]. Without the $\epsilon \ll 1$ assumption, the statistics would cease to be Poissonian [38].

D. Continuous-space limit

It will be convenient to approximate the image-plane modes in a continuous-space limit. Define

$$x_j = x_0 + j \delta x \quad (2.25)$$

as the position of each pixel, and redefine a_j and $|j\rangle$ as

$$a(x_j) \equiv \frac{1}{\sqrt{\delta x}} a_j, \quad |x_j\rangle \equiv a^\dagger(x_j) |\text{vac}\rangle = \frac{1}{\sqrt{\delta x}} |j\rangle, \quad (2.26)$$

such that, for infinitesimal δx ,

$$[a(x), a^\dagger(x')] = \delta(x - x'), \quad \langle x|x'\rangle = \delta(x - x'). \quad (2.27)$$

The single-photon states $|\psi_s\rangle$ defined in Eqs. (2.14) and (2.15) can be rewritten as

$$|\psi_s\rangle = \int_{-\infty}^{\infty} dx \psi_s(x) |x\rangle, \quad s = 1, 2, \quad (2.28)$$

where $\psi_s(x)$ is the continuous limit of $\psi_{ju_s}/\sqrt{\delta x}$ and a configuration-space wavefunction normalized with the standard condition $\int_{-\infty}^{\infty} dx |\psi_s(x)|^2 = 1$. Such definitions are safe in the paraxial regime [19]. For image-plane photon counting, the statistics should be expressed in terms of the mean intensity. Taking the continuous limit of $\Lambda_j/\delta x$, the normalized mean intensity profile becomes

$$\Lambda(x) = \frac{1}{2} [|\psi_1(x)|^2 + |\psi_2(x)|^2]. \quad (2.29)$$

Let us take stock of our formalism thus far. Eq. (2.16) means that a photon arrives with probability ϵ , and it is equally probable that it comes from one source or the other. If the photon comes from the first source, it is in the state $|\psi_1\rangle$ with wavefunction $\psi_1(x)$, otherwise it is in the state $|\psi_2\rangle$ with wavefunction $\psi_2(x)$, as illustrated in Fig. 1(a). Each wavefunction is determined by the field propagation from each source in the imaging system, and the resulting density operator is an incoherent mixture of these possibilities, as one would expect from two incoherent sources. With photon counting on the image plane, the statistics are Poissonian with the mean intensity proportional to Eq. (2.29), as sketched in Fig. 1(b). Note the crucial point that

$$\langle \psi_1 | \psi_2 \rangle = \int_{-\infty}^{\infty} dx \psi_1^*(x) \psi_2(x) \neq 0, \quad (2.30)$$

and the spatial modes excited by the two sources are not orthogonal in general. This overlap underlies all the mathematical and physical difficulties with the problem, as it implies on a fundamental level that the two modes cannot be separated for independent measurements.

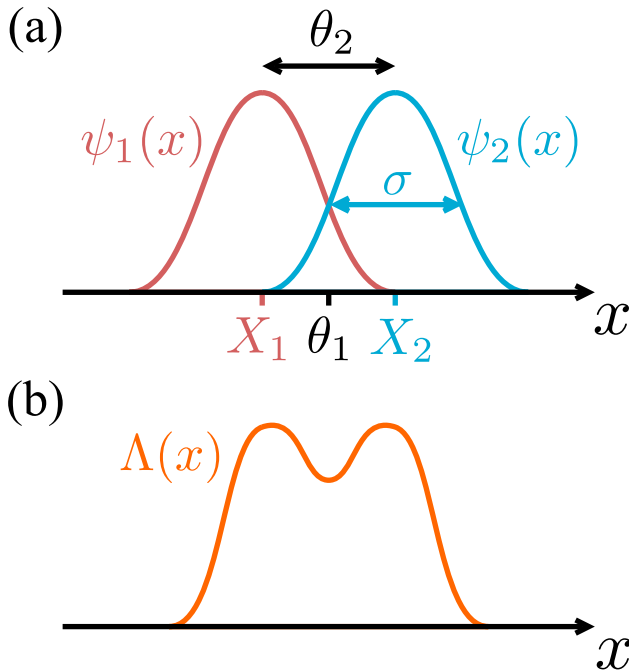


FIG. 1. (a) A cartoon of two photonic wavefunctions on the image plane, each coming from a point source. X_1 and X_2 are the point-source positions, θ_1 is the centroid, θ_2 is the separation, and σ is the width of the point-spread function. (b) If photon counting is performed on the image plane, the statistics are Poissonian with a mean intensity proportional to $\Lambda(x)$, which is the incoherent sum of ψ_1 and ψ_2 .

III. QUANTUM METROLOGY

A. Classical and quantum Cramér-Rao bounds

Photon counting on the image plane is a standard measurement method, but only one of the infinite possibilities allowed by quantum mechanics. The probability distribution of a measurement outcome \mathcal{Y} for any quantum measurement on M copies of an object with ρ can be expressed as

$$P(\mathcal{Y}) = \text{tr} E(\mathcal{Y}) \rho^{\otimes M}, \quad (3.1)$$

where $E(\mathcal{Y})$ is the positive operator-valued measure (POVM) for the measurement, $\rho^{\otimes M}$ denotes the tensor product of M copies of ρ , and tr denotes the operator trace [12, 41]. Suppose that ρ depends on unknown parameters $(\theta_1, \theta_2, \dots, \theta_R)$ and the estimator $\check{\theta}_\mu(\mathcal{Y})$ is constructed from \mathcal{Y} to estimate θ_μ . Define the error covariance matrix as

$$\Sigma_{\mu\nu} \equiv \sum_{\mathcal{Y}} P(\mathcal{Y}) [\check{\theta}_\mu(\mathcal{Y}) - \theta_\mu] [\check{\theta}_\nu(\mathcal{Y}) - \theta_\nu]. \quad (3.2)$$

For any POVM and any unbiased estimator, Σ satisfies the matrix classical and quantum Cramér-Rao bounds [12, 13, 42]

$$\Sigma \geq \mathcal{J}^{-1} \geq \mathcal{K}^{-1}, \quad (3.3)$$

where the matrix inequalities imply that $\Sigma - \mathcal{J}^{-1}$, $\mathcal{J}^{-1} - \mathcal{K}^{-1}$, and also $\Sigma - \mathcal{K}^{-1}$ are positive-semidefinite, \mathcal{J} is the classical Fisher information matrix given by

$$\mathcal{J}_{\mu\nu} = \sum_{\mathcal{Y}} \frac{1}{P(\mathcal{Y})} \frac{\partial P(\mathcal{Y})}{\partial \theta_\mu} \frac{\partial P(\mathcal{Y})}{\partial \theta_\nu}, \quad (3.4)$$

and \mathcal{K} is the quantum Fisher information matrix given by

$$\mathcal{K}_{\mu\nu} = M \text{tr} \frac{\mathcal{L}_\mu \mathcal{L}_\nu + \mathcal{L}_\nu \mathcal{L}_\mu}{2} \rho. \quad (3.5)$$

\mathcal{L}_μ is called the symmetric logarithmic derivative (SLD). Diagonalizing ρ in an orthogonal basis $\{|e_n\rangle\}$ as

$$\rho = \sum_n D_n |e_n\rangle \langle e_n|, \quad (3.6)$$

\mathcal{L}_μ can be expressed as [42, 43]

$$\mathcal{L}_\mu = \sum_{n,m; D_n + D_m \neq 0} \frac{2}{D_n + D_m} \langle e_n | \frac{\partial \rho}{\partial \theta_\mu} | e_m \rangle | e_n \rangle \langle e_m |. \quad (3.7)$$

The calculation of \mathcal{K} for the density operator given by Eq. (2.16) requires a few more assumptions to become tractable.

B. Technical assumptions

Let X_1 and X_2 be the unknown positions of the point sources on the object plane. For later convenience, we define the parameters of interest as the centroid

$$\theta_1 = \frac{X_1 + X_2}{2} \quad (3.8)$$

and the separation

$$\theta_2 = X_2 - X_1, \quad (3.9)$$

as depicted in Fig. 1(a). We assume that the image-plane coordinate x has been divided by the magnification factor of the imaging system to have the same scale as X_μ and the imaging system is spatially invariant, such that the wavefunctions can be expressed in terms of the amplitude point-spread function $\psi(x)$ as

$$\psi_1(x) = \psi(x - X_1), \quad \psi_2(x) = \psi(x - X_2). \quad (3.10)$$

We also assume that $\psi(x)$ is real, viz.,

$$\psi(x) = \psi^*(x). \quad (3.11)$$

It is straightforward to make $\psi_\mu(x)$ spatially invariant and real using two lenses [40], while for other setups we assume that there exists a θ_μ -independent unitary U such that $U\rho U^\dagger$ has a point-spread function that obeys Eqs. (3.10) and (3.11). In other words, we assume that there exists an optical system that can turn the imaging system of interest into an effectively two-lens system; a study of Fourier optics in Ref. [40] should convince the reader that this assumption introduces little loss of generality in the context of linear optical imaging systems. With $\text{tr} E(\mathcal{Y})\rho = \text{tr} E'(\mathcal{Y})U\rho U^\dagger$ and $E'(\mathcal{Y}) = UE(\mathcal{Y})U^\dagger$ being another POVM, any quantum bound derived from $U\rho U^\dagger$ that is valid for arbitrary $E'(\mathcal{Y})$ is also applicable to ρ for arbitrary $E(\mathcal{Y})$. Thus, with little loss of generality, we assume the density operator given by Eq. (2.16), the single-photon states given by Eq. (2.28), and a real and spatially invariant point-spread function according to Eqs. (3.10) and (3.11). With these assumptions, the derivation of the \mathcal{K} matrix according to Eqs. (3.5)–(3.7) remains quite involved and the details are delegated to Appendix A.

C. Error bounds for centroid and separation estimation

The quantum Fisher information matrix \mathcal{K} in terms of the centroid and separation parameters is diagonal and found to be

$$\mathcal{K} = N \begin{pmatrix} 4(\Delta k^2 - \gamma^2) & 0 \\ 0 & \Delta k^2 \end{pmatrix}, \quad (3.12)$$

$$\Delta k^2 \equiv \int_{-\infty}^{\infty} dx \left[\frac{\partial \psi(x)}{\partial x} \right]^2, \quad (3.13)$$

$$\gamma(\theta_2) \equiv \int_{-\infty}^{\infty} dx \frac{\partial \psi(x)}{\partial x} \psi(x - \theta_2). \quad (3.14)$$

Eqs. (3.12)–(3.14) are the first important result of the paper. The prefactor N , the average photon number, indicates the shot-noise scaling expected from classical sources [11, 14]. Δk^2 is the spatial-frequency variance of the point-spread function, while γ^2 depends on θ_2 , the separation between the two sources. For $\theta_2 \rightarrow \infty$, $\gamma^2 \rightarrow 0$, and we recover the standard shot-noise limits for estimating the locations of two isolated sources. For θ_2 on the order of the point-spread function width, γ^2 becomes larger, and the centroid Fisher information \mathcal{K}_{11} experiences a dip. For $\theta_2 \rightarrow 0$, γ^2 vanishes again owing to a real $\psi(x)$, and \mathcal{K}_{11} returns to the original level. \mathcal{K}_{22} , meanwhile, stays constant regardless of θ_2 .

The quantum information can be compared with the classical Fisher information matrix \mathcal{J} in Eq. (3.4) for the image-plane photon-counting statistics governed by Eq. (2.23). In the continuous-space limit,

$$\mathcal{J}_{\mu\nu}^{(\text{ipc})} = N \int_{-\infty}^{\infty} dx \frac{1}{\Lambda(x)} \frac{\partial \Lambda(x)}{\partial \theta_\mu} \frac{\partial \Lambda(x)}{\partial \theta_\nu}, \quad (3.15)$$

where $\Lambda(x)$ is the mean intensity profile given by Eq. (2.29). Alternatively, the exact same result can be derived directly from Eqs. (2.17) and (2.18) without the Poissonian approximation. $\mathcal{J}^{(\text{ipc})}$ also turns out to be diagonal.

Fig. 2 plots the diagonal elements of both $\mathcal{J}^{(\text{ipc})}$ and \mathcal{K} , assuming a Gaussian point-spread function given by

$$\psi(x) = \frac{1}{(2\pi\sigma^2)^{1/4}} \exp\left(-\frac{x^2}{4\sigma^2}\right), \quad \sigma = \frac{\lambda}{2\pi\text{NA}}, \quad (3.16)$$

where λ is the free-space wavelength and NA is the effective numerical aperture. The constant \mathcal{K}_{22} becomes

$$\Delta k = \frac{1}{2\sigma}, \quad \mathcal{K}_{22} = \frac{N}{4\sigma^2}. \quad (3.17)$$

The Gaussian case is representative and the same qualitative behaviors can be observed for other common point-spread functions. Consider first the centroid information quantities \mathcal{K}_{11} and $\mathcal{J}_{11}^{(\text{ipc})}$ plotted in Fig. 2. For $\theta_2 \rightarrow \infty$, they approach the same limit $N/(4\sigma^2)$, indicating that the measurement is near-optimal in determining the centroid of well-separated sources. For smaller θ_2 , both quantities experience dips before recovering towards $\theta_2 = 0$. $\mathcal{J}_{11}^{(\text{ipc})} \leq \mathcal{K}_{11}$ as it should, but the small gap between the two means that there is little room for improvement.

The difference between the separation information quantities \mathcal{K}_{22} and $\mathcal{J}_{22}^{(\text{ipc})}$ in Fig. 2 is much more dramatic. Both quantities approach the same limit $N/(4\sigma^2)$ as $\theta_2 \rightarrow \infty$, implying that the measurement is near-optimal for well-separated sources. For $\theta_2/\sigma \rightarrow 0$, however, the classical information $\mathcal{J}_{22}^{(\text{ipc})}$ decreases to zero. This means that image-plane photon counting is progressively worse at estimating the separation for closer sources, to the point that the information becomes singular and the Cramér-Rao bound diverges at $\theta_2 = 0$.

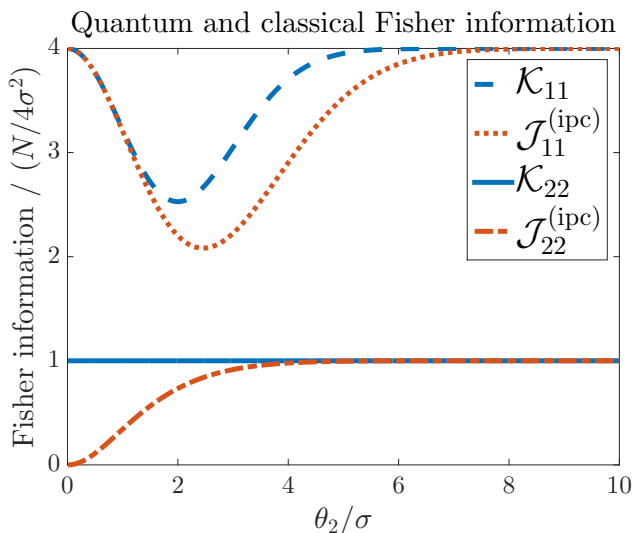


FIG. 2. Plots of Fisher information quantities versus the separation for a Gaussian point-spread function. \mathcal{K}_{11} and \mathcal{K}_{22} are the quantum values for the estimation of the centroid $\theta_1 = (X_1 + X_2)/2$ and the separation $\theta_2 = X_2 - X_1$, respectively, while $\mathcal{J}_{11}^{(\text{ipc})}$ and $\mathcal{J}_{22}^{(\text{ipc})}$ are the corresponding classical values for image-plane photon counting. The horizontal axis is normalized with respect to the point-spread function width σ , while the vertical axis is normalized with respect to $N/(4\sigma^2)$, the value of \mathcal{K}_{22} .

We call the divergent behavior Rayleigh's curse, as it implies that, even though estimation is still possible for any $\theta_2 \neq 0$ and can be improved by increasing the photon number N , there is a severe penalty for a given N when the intensities of the two sources overlap significantly and Rayleigh's criterion is violated. To belabor the point, Fig. 3 plots the quantum and classical Cramér-Rao bounds $1/\mathcal{K}_{22}$ and $1/\mathcal{J}_{22}^{(\text{ipc})}$, demonstrating more dramatically the divergent error in the classical case.

It can be proved that $\mathcal{J}_{22}^{(\text{ipc})}$ must vanish at $\theta_2 = 0$ and Rayleigh's curse exists for image-plane photon counting with any point-spread function. Let

$$I(x) \equiv |\psi(x)|^2 \quad (3.18)$$

be the intensity point-spread function. Then the mean intensity in Eq. (2.29) is

$$\Lambda(x) = I\left(x - \theta_1 + \frac{\theta_2}{2}\right) + I\left(x - \theta_1 - \frac{\theta_2}{2}\right). \quad (3.19)$$

For small θ_2 , we can expand $\Lambda(x)$ to the second order to obtain

$$\Lambda(x) = I(x - \theta_1) + \frac{\theta_2^2}{4} \frac{\partial^2 I(x - \theta_1)}{\partial x^2} + o(\theta_2^2), \quad (3.20)$$

where $o(\theta_2^2)$ denotes terms asymptotically smaller than θ_2^2 . Substituting this into Eq. (3.15) gives

$$\mathcal{J}_{22}^{(\text{ipc})} = \frac{\theta_2^2 N}{4} \int_{-\infty}^{\infty} dx \frac{1}{I(x)} \left[\frac{\partial^2 I(x)}{\partial x^2} \right]^2 + o(\theta_2^2), \quad (3.21)$$

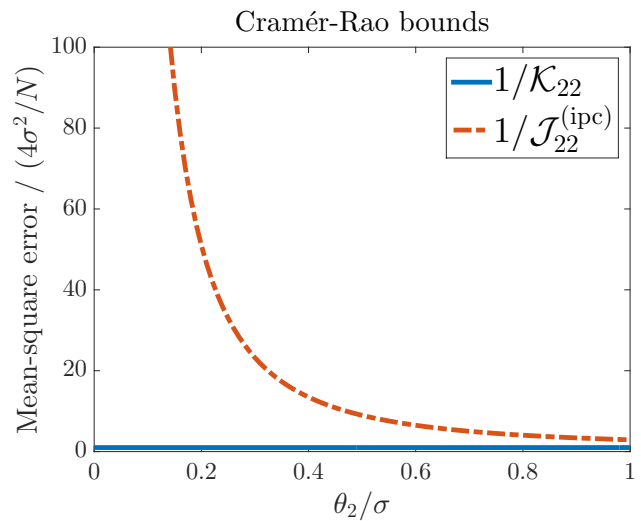


FIG. 3. Quantum ($1/\mathcal{K}_{22}$) and classical ($1/\mathcal{J}_{22}^{(\text{ipc})}$) Cramér-Rao bounds versus normalized separation θ_2/σ for a Gaussian point-spread function. The bounds are normalized with respect to the quantum value $4\sigma^2/N$. Rayleigh's curse refers to the divergence of the classical bound.

which is zero for $\theta_2 = 0$. This singularity is the reason why the resolution measure proposed by Ram *et al.* in terms of separation estimation diverges for $\theta_2 \rightarrow 0$ [8].

Remarkably, the quantum information \mathcal{K}_{22} stays constant regardless of the separation. If the centroid θ_1 is known, there exists a quantum measurement to make the single-parameter QCRB

$$\Sigma_{22} \geq \frac{1}{\mathcal{K}_{22}} = \frac{1}{N\Delta k^2} \quad (3.22)$$

asymptotically attainable for large M , as proved by Fujiwara [15]. This means that, at least in principle, Rayleigh's curse can be avoided for separation estimation, and considerable improvements can be obtained, if the optimal quantum measurement can be implemented.

IV. SPATIAL-MODE DEMULTIPLEXING (SPADE)

A. Hermite-Gaussian modes

In the photonic configuration-space picture, image-plane photon counting is a measurement in the photonic position basis $\{|x\rangle; x \in (-\infty, \infty)\}$. For another possibility, consider the discrete Hermite-Gaussian basis $\{|\phi_q\rangle; q = 0, 1, \dots\}$, where

$$|\phi_q\rangle = \int_{-\infty}^{\infty} dx \phi_q(x) |x\rangle, \quad q = 0, 1, \dots \quad (4.1)$$

$$\phi_q(x) = \left(\frac{1}{2\pi\sigma^2}\right)^{1/4} \frac{1}{\sqrt{2^q q!}} H_q\left(\frac{x}{\sqrt{2}\sigma}\right) \exp\left(-\frac{x^2}{4\sigma^2}\right), \quad (4.2)$$

and H_q is the Hermite polynomial [44]. The full POVM for each trial can be expressed as projections

$$E_0 = |\text{vac}\rangle\langle\text{vac}|, \quad E_1(q) = |\phi_q\rangle\langle\phi_q|, \quad (4.3)$$

and the outcome probabilities for the state in Eq. (2.16) become

$$P_0 \equiv \text{tr } E_0 \rho = 1 - \epsilon, \quad (4.4)$$

$$P_1(q) \equiv \text{tr } E_1(q) \rho = \frac{\epsilon}{2} \left(|\langle\phi_q|\psi_1\rangle|^2 + |\langle\phi_q|\psi_2\rangle|^2 \right). \quad (4.5)$$

To proceed further, we assume that the centroid θ_1 is known, and only θ_2 is to be estimated. Since centroid estimation using image-plane photon counting is relatively insensitive to the separation, the assumption of a known centroid is not difficult to satisfy. Let $\theta_1 = 0$ without loss of generality, and the wavefunctions become

$$\psi_1(x) = \psi\left(x + \frac{\theta_2}{2}\right), \quad \psi_2(x) = \psi\left(x - \frac{\theta_2}{2}\right). \quad (4.6)$$

For simple analytic results, we further assume that the point-spread function is Gaussian, viz.,

$$\psi(x) = \phi_0(x). \quad (4.7)$$

The overlap factors in Eq. (4.5) become

$$|\langle\phi_q|\psi_1\rangle|^2 = \left| \int_{-\infty}^{\infty} dx \phi_q^*(x) \phi_0\left(x + \frac{\theta_2}{2}\right) \right|^2, \quad (4.8)$$

$$|\langle\phi_q|\psi_2\rangle|^2 = \left| \int_{-\infty}^{\infty} dx \phi_q^*(x) \phi_0\left(x - \frac{\theta_2}{2}\right) \right|^2. \quad (4.9)$$

We can evaluate them by recognizing that $|\phi_q\rangle$ is mathematically equivalent to an energy eigenstate of a harmonic oscillator (in the configuration space of the photon), and $|\psi_1\rangle$ and $|\psi_2\rangle$ are equivalent to configuration-space coherent states with displacements $\pm\theta_2/(4\sigma)$. The result is a Poissonian distribution given by

$$|\langle\phi_q|\psi_1\rangle|^2 = |\langle\phi_q|\psi_2\rangle|^2 = \exp(-Q) \frac{Q^q}{q!}, \quad (4.10)$$

$$Q \equiv \frac{\theta_2^2}{16\sigma^2}. \quad (4.11)$$

Hence

$$P_1(q) = \epsilon \exp(-Q) \frac{Q^q}{q!}. \quad (4.12)$$

As $|\langle\phi_q|\psi_1\rangle|^2 = |\langle\phi_q|\psi_2\rangle|^2$, this formula is valid even if the two sources have unequal intensities and ρ is any mixture of $|\text{vac}\rangle\langle\text{vac}|$, $|\psi_1\rangle\langle\psi_1|$, and $|\psi_2\rangle\langle\psi_2|$ with zero-photon probability $1 - \epsilon$. The classical Fisher information for the Hermite-Gaussian-basis measurement over M trials becomes

$$\begin{aligned} \mathcal{J}_{22}^{(\text{HG})} &= M \sum_{q=0}^{\infty} P_1(q) \left[\frac{\partial}{\partial \theta_2} \ln P_1(q) \right]^2 \\ &= \frac{M\epsilon}{Q} \left(\frac{\partial Q}{\partial \theta_2} \right)^2 = \frac{N}{4\sigma^2} = \mathcal{K}_{22}, \end{aligned} \quad (4.13)$$

which is precisely the quantum information given by Eq. (3.17) and also independent of the separation θ_2 . This proves that the Hermite-Gaussian-basis measurement is quantum-optimal for a Gaussian point-spread function and free of Rayleigh's curse. This is the second important result of the paper.

Suppose that a total of L photons are detected over the M trials. A record of the modes for the L photons (q_1, q_2, \dots, q_L) can be obtained, but in fact a time-resolved record is not necessary, as $\sum_l q_l$ is a sufficient statistic for estimating Q and θ_2 [10], meaning that the set of photon numbers $\{m_q = \sum_l \delta_{qq_l}; q = 0, 1, \dots\}$ detected in different modes are also sufficient. The maximum-likelihood estimator becomes

$$\check{Q}_{\text{ML}} = \frac{1}{L} \sum_q q m_q, \quad \check{\theta}_{2\text{ML}} = 4\sigma \sqrt{\check{Q}_{\text{ML}}}. \quad (4.14)$$

For $L = 0$, one can set $\check{\theta}_2$ to a constant value. Since L is binomial [10], the $L = 0$ probability $(1 - \epsilon)^M \approx \exp(-N)$ is negligible for large N .

Maximum-likelihood estimation can asymptotically saturate the Cramér-Rao bound $\Sigma_{22} \geq 1/\mathcal{J}_{22}^{(\text{HG})}$ for large M [10]. With $\mathcal{J}_{22}^{(\text{HG})} = \mathcal{K}_{22}$, the QCRB in Eq. (3.22) is asymptotically attainable as well. Appendix B reports a Monte-Carlo analysis of maximum-likelihood estimation for finite L and finds that the error is reasonably close to the Cramér-Rao bound, supporting the asymptotic arguments.

B. Multimode-waveguide SPADE

To measure in the Hermite-Gaussian basis according to Eqs. (4.3), one needs to separate the image-plane field in terms of the desired spatial modes, before determining the outcome q based on the mode in which the photon is detected. To do so, one should perform a one-to-one conversion of the Hermite-Gaussian modes into modes in a more accessible degree of freedom. To achieve a high information-extraction efficiency, it is important that the conversion is performed with minimal loss. Here we explore some of the schemes that can in principle be lossless.

We can take advantage of the fact that the Hermite-Gaussian modes are waveguide modes of a quadratic-index waveguide [44]. Suppose that we couple the image-plane optical field into such a highly multimode waveguide centered at the centroid position, as shown in Fig. 4. Each mode acquires a different propagation constant β_q along the longitudinal direction z . If a grating coupler [45] with spatial frequency κ is then used to couple all the modes into free space, each mode will be coupled to a plane wave with a different spatial frequency $\beta_q - \kappa$ along the z direction in free space, and a Fourier-transform lens can be used to focus the different plane waves onto different spots of a photon-counting array in the far field.

An alternative is to use evanescent coupling with different single-mode waveguides [46], as depicted in Fig. 4.

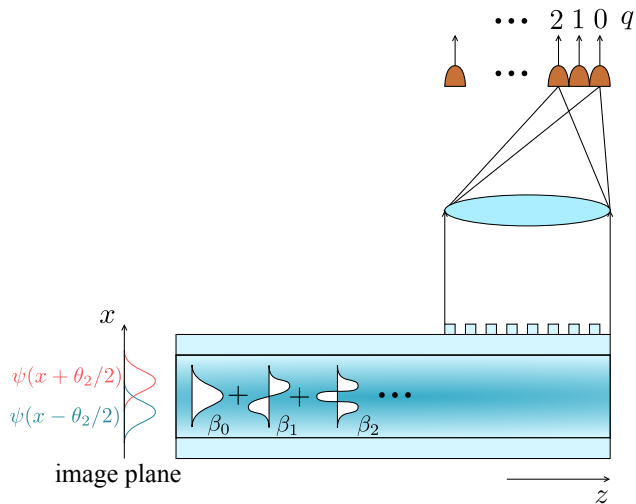


FIG. 4. A multimode-waveguide SPADE with a grating output coupler and far-field photon counting.

If each single-mode waveguide is fabricated to have a propagation constant equal to a different value of β_q , the phase-matching condition will cause each mode in the multimode waveguide to be coupled to a specific fiber.

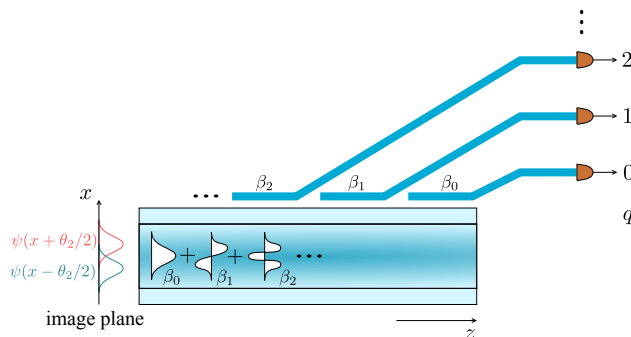


FIG. 5. A multimode-waveguide SPADE with evanescent coupling to single-mode waveguides with different propagation constants for phase matching.

Given these physical setups, the sensitivity of SPADE can be explained in a more intuitive semiclassical optics language: it results from the exquisite sensitivity of the mode-coupling efficiencies to the offset of the point-spread function. The incoherent sources are literally blinking on the fundamental coherence time scale, causing each image-plane photon to have a wavefunction given randomly by $\psi_1(x)$ or $\psi_2(x)$. Either wavefunction can excite the waveguide modes coherently, and the excitation probabilities are sensitive to the offset but oblivious to which source the photon comes from. The classical randomness has no effect on the final measurement statistics as a result.

Practical issues such as mode mismatch, imperfect coupling efficiencies, crosstalk, finite number of modes, and optical losses will impact the realistic performance of the devices. However, given the quantum-optimal perfor-

mance that they can theoretically achieve and the fundamental inability of image-plane photon counting to resolve close point sources, the potential of SPADE remains significant.

C. Binary SPADE

Since image-plane photon counting has trouble estimating the separation only when θ_2/σ is small, and Eq. (4.12) suggests that the excitation of a Hermite-Gaussian mode is significant only when $q \sim \theta_2^2/(16\sigma^2)$, we can focus on the situation where θ_2/σ is small and only the low-order modes need to be discriminated to simplify the SPADE design. One such design is depicted in Fig. 6, where only the $q = 0$ component is coupled into the single-mode waveguide, while any photon in the higher-order modes remains in the multimode waveguide for subsequent detection.

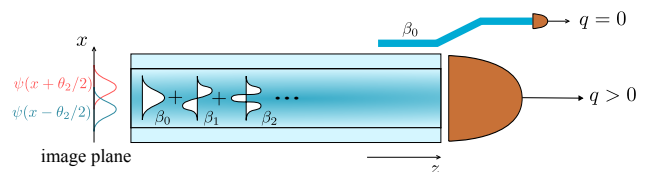


FIG. 6. Binary SPADE with evanescent coupling to only one single-mode waveguide.

An alternative design for binary SPADE using a single-mode waveguide is depicted in Fig. 7. The single-mode waveguide is coupled to the zeroth-order mode $q = 0$ only, while higher-order modes are necessarily coupled to the leaky modes of the waveguide, which are also measured.

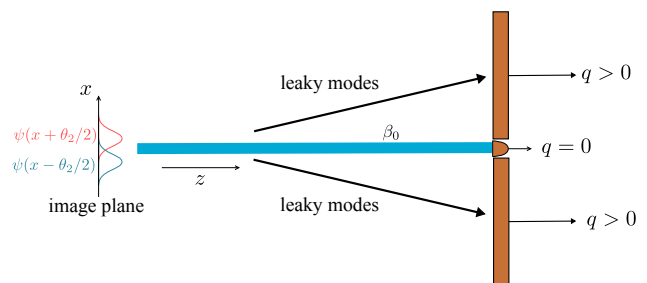


FIG. 7. Binary SPADE via a single-mode waveguide and leaky-mode detection.

The probability of detecting a photon in the $q = 0$ mode remains

$$P_1(q = 0) = \epsilon \exp(-Q), \quad (4.15)$$

but now the higher-order modes cannot be discriminated, and the probability of detecting a photon in any higher-order mode becomes

$$P_1(q > 0) = \epsilon [1 - \exp(-Q)]. \quad (4.16)$$

The Fisher information for this scheme is

$$\mathcal{J}_{22}^{(b)} = \frac{N}{4\sigma^2} \frac{Q \exp(-Q)}{1 - \exp(-Q)}. \quad (4.17)$$

Fig. 8 compares $\mathcal{J}_{22}^{(b)}$ with $\mathcal{J}_{22}^{(\text{HG})} = \mathcal{K}_{22}$ as well as $\mathcal{J}_{22}^{(\text{ipc})}$ for image-plane photon counting. It can be seen that binary SPADE gives significant information for small θ_2/σ , where image-plane photon counting performs poorly. Binary SPADE actually works less well when the sources are far apart, and the two methods can complement each other.

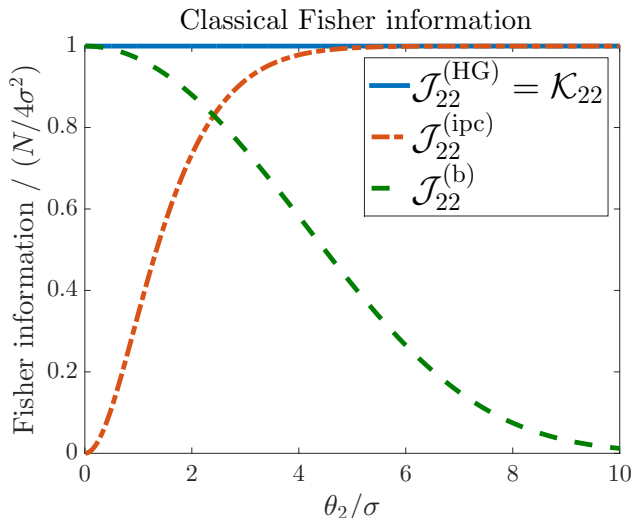


FIG. 8. Fisher information for the estimation of θ_2 with different schemes versus normalized separation θ_2/σ for a Gaussian point-spread function. $\mathcal{J}_{22}^{(\text{HG})}$ is the information for the ideal Hermite-Gaussian-basis measurement, which is equal to the quantum value \mathcal{K}_{22} , $\mathcal{J}_{22}^{(\text{ipc})}$ is for image-plane photon counting, and $\mathcal{J}_{22}^{(b)}$ is for binary SPADE. The vertical axis is normalized with respect to $\mathcal{J}_{22}^{(\text{HG})} = \mathcal{K}_{22} = N/(4\sigma^2)$.

For a total of L detected photons, m_0 , the number of photons detected in the $q = 0$ mode, is a sufficient statistic for estimating Q and θ_2 and follows the binomial distribution with success probability $\exp(-Q)$ [10]. The maximum-likelihood estimator becomes

$$\check{Q}_{\text{ML}}^{(b)} = -\ln \frac{m_0}{L}, \quad \check{\theta}_{2\text{ML}}^{(b)} = 4\sigma \sqrt{\check{Q}_{\text{ML}}^{(b)}}. \quad (4.18)$$

For $L = 0$ or $m_0 = 0$, one can select finite values for $\check{\theta}_2$ to regularize the estimator. Appendix B reports a Monte-Carlo analysis of this estimator for finite L , supporting our use of the Fisher information measure to represent the performance of binary SPADE.

Compared with the large amount of data generated by image-plane photon counting and the complex algorithms needed to process them, only two numbers L and m_0 are needed here. The highly compressed measurement output, enabled by coherent linear optical processing, is a bonus for binary SPADE or its higher-order generalizations.

D. Other point-spread functions

Our analysis of SPADE so far relies on the assumption of a Gaussian point-spread function. For other point-spread functions, it is nontrivial to find a suitable basis of spatial modes. If we can fabricate a single-mode waveguide with a mode profile that matches the point-spread function $\psi(x)$, however, the analysis of the binary SPADE in Fig. 7 is still tractable. Again let $\theta_1 = 0$ without loss of generality. Define

$$|\psi\rangle = \int_{-\infty}^{\infty} dx \psi(x) |x\rangle \quad (4.19)$$

as the state of one photon in the waveguide mode. The efficiency of coupling a photon in state $|\psi_1\rangle$ or $|\psi_2\rangle$ into the waveguide mode becomes

$$|\langle\psi|\psi_1\rangle|^2 = |\langle\psi|\psi_2\rangle|^2 \quad (4.20)$$

$$= \left| \int_{-\infty}^{\infty} dx \psi^*(x) \psi \left(x + \frac{\theta_2}{2} \right) \right|^2 \quad (4.21)$$

$$= \left| \int_{-\infty}^{\infty} dk |\Psi(k)|^2 \exp\left(\frac{ik\theta_2}{2}\right) \right|^2 \quad (4.22)$$

$$\equiv \Gamma(\theta_2), \quad (4.23)$$

where $\Gamma(\theta_2)$ is the mode overlap factor and

$$\Psi(k) \equiv \int_{-\infty}^{\infty} \frac{dx}{\sqrt{2\pi}} \psi(x) \exp(-ikx) \quad (4.24)$$

is the optical transfer function of the imaging system before the image plane [40]. For the density operator in Eq. (2.16), or in fact any density operator in a mixture of $|\text{vac}\rangle\langle\text{vac}|$, $|\psi_1\rangle\langle\psi_1|$, and $|\psi_2\rangle\langle\psi_2|$ with zero-photon probability $1 - \epsilon$, the probability of finding a photon in the waveguide mode becomes

$$P_1(\psi) = \epsilon\Gamma, \quad (4.25)$$

and the probability of finding a photon in any other mode is

$$P_1(\bar{\psi}) = \epsilon(1 - \Gamma). \quad (4.26)$$

The Fisher information over M trials is then

$$\mathcal{J}_{22}^{(b)} = \frac{N}{\Gamma(1 - \Gamma)} \left(\frac{\partial\Gamma}{\partial\theta_2} \right)^2. \quad (4.27)$$

To study its behavior for small θ_2 , expand $\Gamma(\theta_2)$ in Eq. (4.22) as

$$\Gamma(\theta_2) \approx 1 - \frac{\Delta k^2}{4} \theta_2^2, \quad (4.28)$$

$$\Delta k^2 = \int_{-\infty}^{\infty} dk |\Psi(k)|^2 k^2 - \left[\int_{-\infty}^{\infty} dk |\Psi(k)|^2 k \right]^2, \quad (4.29)$$

giving

$$\mathcal{J}_{22}^{(b)}(\theta_2 = 0) = N\Delta k^2 = \mathcal{K}_{22}. \quad (4.30)$$

For a real point-spread function, $\mathcal{J}_{22}^{(b)}$ can hence reach the quantum information \mathcal{K}_{22} in Eq. (3.12) at $\theta_2 = 0$, precisely where $\mathcal{J}_{22}^{(\text{ipc})}$ vanishes according to Eq. (3.21) and Rayleigh's curse is at its worst. For larger θ_2 , $\mathcal{J}_{22}^{(b)}$ is expected to decrease, as the scheme is unable to discriminate the higher-order modes that become more likely to be occupied. Fig. 9 plots \mathcal{K}_{22} , the numerically computed $\mathcal{J}_{22}^{(\text{ipc})}$, and $\mathcal{J}_{22}^{(b)}$ for the sinc point-spread function

$$\psi(x) = \frac{1}{\sqrt{W}} \text{sinc}\left(\frac{x}{W}\right), \quad W = \frac{\lambda}{2\text{NA}}, \quad (4.31)$$

where $\text{sinc } u \equiv \sin(\pi u)/(\pi u)$. The information quantities demonstrate behaviors similar to the Gaussian case shown in Fig. 8.

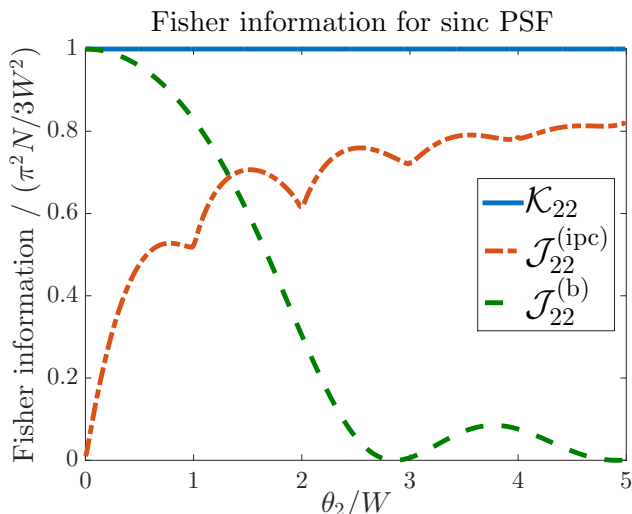


FIG. 9. Fisher information quantities versus normalized separation θ_2/W for the sinc point-spread function. \mathcal{K}_{22} is the quantum value, $\mathcal{J}_{22}^{(\text{ipc})}$ is the numerically computed value for image-plane photon counting, and $\mathcal{J}_{22}^{(b)}$ is that for binary SPADE tailored for the sinc function. The vertical axis is normalized with respect to $\mathcal{K}_{22} = \pi^2 N/(3W^2)$.

V. TWO-DIMENSIONAL IMAGING

The essential physics remains unchanged when we consider two-dimensional imaging, and we discuss the generalization only briefly. The single-photon states in Eq. (2.16) should now be expressed as

$$|\psi_s\rangle = \int_{-\infty}^{\infty} dx \int_{-\infty}^{\infty} dy \psi_s(x, y) |x, y\rangle, \quad s = 1, 2, \quad (5.1)$$

where $\langle x, y|x', y'\rangle = \delta(x - x')\delta(y - y')$ and $\psi_s(x, y)$ is a two-dimensional wavefunction [19]. In terms of a point-spread function $\psi(x, y)$ and unknown positions (X_1, Y_1) and (X_2, Y_2) ,

$$\psi_s(x, y) = \psi(x - X_s, y - Y_s), \quad (5.2)$$

and we can define the four centroid and separation parameters as

$$\theta_{1X} = \frac{X_1 + X_2}{2}, \quad \theta_{1Y} = \frac{Y_1 + Y_2}{2}, \quad (5.3)$$

$$\theta_{2X} = X_2 - X_1, \quad \theta_{2Y} = Y_2 - Y_1. \quad (5.4)$$

$\mathcal{J}^{(\text{ipc})}$ for the estimation of θ_{2X} and θ_{2Y} decreases to zero when the sources are close, and Rayleigh's curse still exists for image-plane photon counting [8]. The quantum Fisher information matrix is even more tedious to work out and will not be attempted here.

An analysis of SPADE is fortunately still tractable. Assuming a Gaussian point-spread function and a known centroid, it is straightforward to show that measurements in the two-dimensional Hermite-Gaussian basis with mode numbers q and p give rise to Poissonian statistics for the measurement outcomes $(q_1, p_1, q_2, p_2, \dots, q_L, p_L)$ with L detected photons, and the classical Fisher information with respect to θ_{2X} and θ_{2Y} remains a constant and free of Rayleigh's curse, similar to the one-dimensional case. For other point-spread functions, such as the Airy disk [2, 40], binary SPADE with a matching mode profile can estimate the separation without Rayleigh's curse for small separations in the same way as that described in Sec. IV D, but information about the direction of the separation is lost. To obtain directional information, one needs to discriminate at least some of the higher-order modes in different directions.

A quadratic-index optical fiber can support Hermite-Gaussian modes, while a weakly guiding step-index fiber also has modes closely resembling the Hermite-Gaussian modes [45]. A complication arises for cylindrically symmetric fibers, as modes with the same total order $q+p$ will have a degenerate propagation constant, causing multiple modes to satisfy the same phase-matching conditions in grating or evanescent coupling and preventing discrimination of modes with the same order. The net result is that directional information is compromised. One solution is to turn the point-spread function into an elliptic one with asymmetric widths and use an elliptic fiber to break the degeneracy.

VI. CONCLUSION

We have presented two important results in this paper: the QCRB for locating two incoherent optical point sources, and the SPADE measurement method for quantum-optimal separation estimation. The QCRB for separation estimation can be significantly lower than the classical bound for image-plane photon counting, and

SPADE can extract the full information offered by quantum mechanics via coherent linear optical processing. The proposed SPADE and binary SPADE schemes work well for close sources with significant overlap in their wavefunctions, avoiding Rayleigh's curse and the divergent error that plagues image-plane photon counting [8]. The highly compressed measurement output of binary SPADE is a bonus.

Further investigations are needed to study the issues of more spatial and spectral dimensions, more sources, polarization and nonparaxial effects, background noise, turbulence, optical loss, mode mismatch, crosstalk, and dark counts. These issues, while important for practical applications, do not detract from the central message of our work: Rayleigh's criterion is fundamentally irrelevant to incoherent-point-source localization at optical frequencies. It proves to be a curse of technical nature specific to a conventional imaging method, and cleverer quantum measurements, such as SPADE, can locate two close incoherent sources from far field almost as accurately as conventional methods do for isolated sources.

AUTHOR CONTRIBUTIONS

M. T. developed the formalism in Sec. II. R. N. derived the quantum bound in Sec. III and Appendix A, with X. L. and M. T.'s inputs and checks. M. T. invented the measurement methods in Sec. IV, explored the two-dimensional case in Sec. V, performed the numerical analysis in Appendix B, and wrote the paper. All authors discussed extensively during the course of this work.

ACKNOWLEDGMENTS

Helpful discussions with Shan Zheng Ang and Shilin Ng are gratefully acknowledged. This work is supported by the Singapore National Research Foundation under NRF Grant No. NRF-NRFF2011-07.

Appendix A: Quantum Fisher information matrix

To compute the quantum Fisher information matrix given by Eqs. (3.12)–(3.14), we first need to diagonalize ρ as in Eq. (3.6), noting that the eigenvectors should span the support of $\partial\rho/\partial\theta_\mu$. The partial derivative of ρ with respect to X_μ can be expressed as

$$\frac{\partial\rho}{\partial X_\mu} = \frac{\partial D_1}{\partial X_\mu} |e_1\rangle\langle e_1| + \frac{\partial D_2}{\partial X_\mu} |e_2\rangle\langle e_2| + \left[D_1 \frac{\partial |e_1\rangle}{\partial X_\mu} \langle e_1| + D_2 \frac{\partial |e_2\rangle}{\partial X_\mu} \langle e_2| + \text{H.c.} \right], \quad (\text{A1})$$

where H.c. denotes the Hermitian conjugate. In addition to the support of ρ spanned by $|e_0\rangle$, $|e_1\rangle$, and $|e_2\rangle$, we also

need to find more eigenvectors that span the support of $\partial |e_1\rangle/\partial X_\mu$ and $\partial |e_2\rangle/\partial X_\mu$.

Assuming that $\psi_\mu(x) = \psi(x - X_\mu)$ and the point-spread function $\psi(x)$ is real, it can be shown after elaborate algebra that the relevant eigenvectors are

$$\begin{aligned} |e_0\rangle &= |\text{vac}\rangle\langle \text{vac}|, \\ |e_1\rangle &= \frac{1}{\sqrt{2(1-\delta)}} (|\psi_1\rangle - |\psi_2\rangle), \\ |e_2\rangle &= \frac{1}{\sqrt{2(1+\delta)}} (|\psi_1\rangle + |\psi_2\rangle), \\ |e_3\rangle &= \frac{1}{c_3} \left[\Delta k (|\psi_{11}\rangle + |\psi_{22}\rangle) - \frac{2\gamma}{\sqrt{2(1-\delta)}} |e_1\rangle \right], \\ |e_4\rangle &= \frac{1}{c_4} \left[\Delta k (|\psi_{11}\rangle - |\psi_{22}\rangle) + \frac{2\gamma}{\sqrt{2(1+\delta)}} |e_2\rangle \right], \end{aligned} \quad (\text{A2})$$

where Δk is given by Eq. (3.13), γ is given by Eq. (3.14),

$$|\psi_{11}\rangle \equiv \frac{1}{\Delta k} \int_{-\infty}^{\infty} dx \frac{\partial\psi(x - X_1)}{\partial X_1} |x\rangle, \quad (\text{A3})$$

$$|\psi_{22}\rangle \equiv \frac{1}{\Delta k} \int_{-\infty}^{\infty} dx \frac{\partial\psi(x - X_2)}{\partial X_2} |x\rangle, \quad (\text{A4})$$

$$\delta \equiv \int_{-\infty}^{\infty} dx \psi(x - X_1) \psi(x - X_2), \quad (\text{A5})$$

$$c_3 \equiv \left(\Delta k^2 + b^2 - \frac{\gamma^2}{1-\delta} \right)^{1/2}, \quad (\text{A6})$$

$$c_4 \equiv \left(\Delta k^2 - b^2 - \frac{\gamma^2}{1+\delta} \right)^{1/2}, \quad (\text{A7})$$

$$b^2 \equiv \int_{-\infty}^{\infty} dx \frac{\partial\psi(x - X_1)}{\partial X_1} \frac{\partial\psi(x - X_2)}{\partial X_2}, \quad (\text{A8})$$

and the eigenvalues of ρ are

$$\begin{aligned} D_0 &= 1 - \epsilon, & D_1 &= \epsilon \frac{1-\delta}{2}, & D_2 &= \epsilon \frac{1+\delta}{2}, \\ D_3 &= D_4 = 0. \end{aligned} \quad (\text{A9})$$

After more algebra, the SLD in Eq. (3.7) with respect to the derivative in Eq. (A1) can be expressed as

$$\mathcal{L}_\mu^{(X)} = \sum_{n,m} \mathcal{L}_{\mu,nm}^{(X)} |e_n\rangle\langle e_m| \quad (\text{A10})$$

with a real and symmetric matrix $\mathcal{L}_{\mu,nm}^{(X)} = \mathcal{L}_{\mu,mn}^{(X)}$, the nonzero and unique elements of which are found to be

$$\begin{aligned} \mathcal{L}_{1,11}^{(X)} &= -\mathcal{L}_{2,11}^{(X)} = \gamma/(1-\delta), \\ \mathcal{L}_{1,12}^{(X)} &= \mathcal{L}_{2,12}^{(X)} = \gamma\delta/\sqrt{1-\delta^2}, \\ \mathcal{L}_{1,13}^{(X)} &= -\mathcal{L}_{2,13}^{(X)} = c_3/\sqrt{1-\delta}, \\ \mathcal{L}_{1,14}^{(X)} &= \mathcal{L}_{2,14}^{(X)} = c_4/\sqrt{1-\delta}, \\ \mathcal{L}_{1,22}^{(X)} &= -\mathcal{L}_{2,22}^{(X)} = -\gamma/(1+\delta), \\ \mathcal{L}_{1,23}^{(X)} &= \mathcal{L}_{2,23}^{(X)} = c_3/\sqrt{1+\delta}, \\ \mathcal{L}_{1,24}^{(X)} &= -\mathcal{L}_{2,24}^{(X)} = c_4/\sqrt{1+\delta}. \end{aligned} \quad (\text{A11})$$

In terms of the centroid and separation parameters given by Eqs. (3.8) and (3.9), the SLDs become

$$\mathcal{L}_1 = \mathcal{L}_1^{(X)} + \mathcal{L}_2^{(X)}, \quad \mathcal{L}_2 = \frac{\mathcal{L}_2^{(X)} - \mathcal{L}_1^{(X)}}{2}. \quad (\text{A12})$$

We can now substitute Eqs. (A9)–(A12) into Eq. (3.5) to compute the quantum Fisher information matrix. The final result is Eqs. (3.12)–(3.14).

Appendix B: Monte-Carlo analysis of SPADE and binary SPADE with maximum-likelihood estimation

Since the total number of detected photons L is known after an experiment, we can refine our error analysis by conditioning on L rather than the average photon number N . It is not difficult to show that, conditioned on L , the classical and quantum Fisher information in Eqs. (3.12) and (4.13) retain their expressions except that N is replaced by L . The error bounds become

$$\frac{1}{\mathcal{J}_{22}^{(\text{HG})}} = \frac{1}{\mathcal{K}'_{22}} = \frac{4\sigma^2}{L}. \quad (\text{B1})$$

As the sufficient statistic $\sum_q qm_q$ in the maximum-likelihood estimator for SPADE in Eq. (4.14) is Poissonian with mean LQ , it becomes a simple matter to generate numerical simulations of the maximum-likelihood estimates \hat{Q}_{ML} and $\hat{\theta}_{2\text{ML}}$ in Eq. (4.14).

Fig. 10 plots the simulated mean-square errors, normalized with respect to Eq. (B1), for several values of L . It is intriguing to see that, as $\theta_2/\sigma \rightarrow 0$, the errors go below the bounds. This super-efficiency is a well known statistical phenomenon, as the maximum-likelihood estimation of θ_2 is actually biased for finite samples, and the Cramér-Rao bounds need not apply.

To analyze biased estimators, a better way is to use Bayesian bounds [9, 12], which are applicable to the global estimation error of any biased or unbiased estimator. A global estimation error is obtained by averaging the frequentist error considered here over a prior distribution of θ_2 . With the constant Fisher information quantities in Eq. (B1), the Bayesian bounds are equal to their frequentist counterparts in the limit of negligible prior information. The limited rise and fall of the errors shown in Fig. 10 suggest that the global errors should remain close to the Bayesian bounds.

For our purpose, the main point of Fig. 10 is that the errors remain less than twice the Cramér-Rao bounds and even offer the pleasant surprise of super-efficiency for

small separations, thus supporting our use of the Fisher information measures to represent the performance of SPADE. The vanishing information for image-plane photon counting shown in Fig. 2, on the other hand, implies that its Bayesian version will suffer similarly when the prior distribution of θ_2 is concentrated at small θ_2/σ , and any estimator, biased or unbiased, cannot violate the Bayesian bound and must suffer as well.

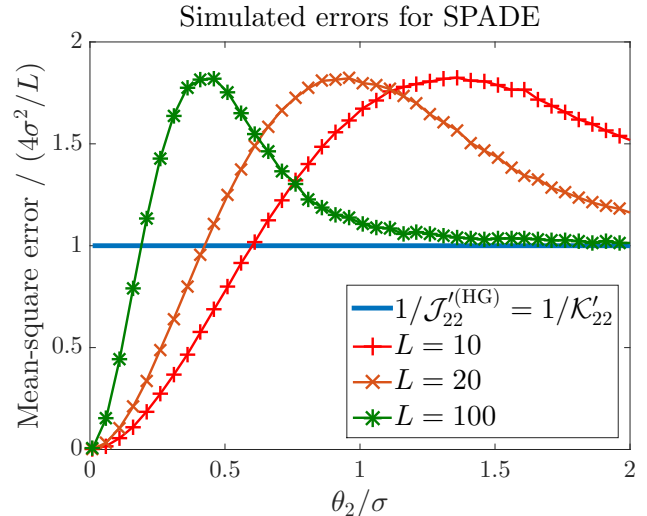


FIG. 10. Simulated mean-square errors of SPADE with maximum-likelihood estimation, conditioned on L detected photons. Note that the vertical axis is normalized with respect to $4\sigma^2/L$, so the plotted values are the actual errors magnified by $L/4\sigma^2$. Each error is computed by averaging 10^5 simulations, and the lines connecting the data points are guides for eyes.

For binary SPADE, the Fisher information conditioned on L has the same form as Eq. (4.17), and the Cramér-Rao bound can be expressed as

$$\frac{1}{\mathcal{J}_{22}^{(\text{b})}} = \frac{4\sigma^2}{L} \frac{1 - \exp(-Q)}{Q \exp(-Q)}. \quad (\text{B2})$$

The sufficient statistic m_0 in $\check{\theta}_{2\text{ML}}^{(\text{b})}$ given by Eq. (4.18) is binomial and also simple to generate. In case $m_0 = 0$, we set $\check{\theta}_2 = 2\sigma$, the maximum of our considered range of θ_2 . Fig. 11 plots the simulated mean-square errors for binary SPADE with otherwise the same parameters as those for Fig. 10. For small θ_2/σ , The errors follow very similar trends as their counterparts in Fig. 10, and for larger θ_2/σ the errors begin to follow the rising Cramér-Rao bound according to Eq. (B2), especially for $L = 100$. This supports our use of the Fisher information to represent the performance of binary SPADE.

[1] Lord Rayleigh, “XXXI. Investigations in optics, with special reference to the spectroscope,” *Philosophical Maga-*

zine Series 5 8, 261–274 (1879).

[2] Max Born and Emil Wolf, *Principles of Optics: Elec-*

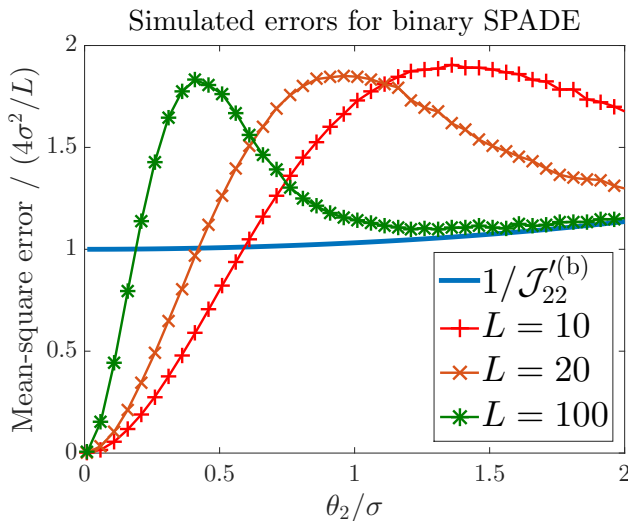


FIG. 11. Simulated mean-square errors for binary SPADE with maximum-likelihood estimation, conditioned on L detected photons. The vertical axis is normalized with respect to $4\sigma^2/L$. Each error is computed by averaging 10^5 simulations, and the lines connecting the data points are guides for eyes.

tromagnetic Theory of Propagation, Interference and Diffraction of Light (Cambridge University Press, Cambridge, 1999).

- [3] Stefan W. Hell and Jan Wichmann, “Breaking the diffraction resolution limit by stimulated emission: stimulated-emission-depletion fluorescence microscopy,” *Opt. Lett.* **19**, 780–782 (1994).
- [4] Eric Betzig, “Proposed method for molecular optical imaging,” *Opt. Lett.* **20**, 237–239 (1995).
- [5] Stefan W. Hell, “Far-field optical nanoscopy,” *Science* **316**, 1153–1158 (2007).
- [6] Eric Betzig, George H. Patterson, Rachid Sougrat, O. Wolf Lindwasser, Scott Olenych, Juan S. Bonifacino, Michael W. Davidson, Jennifer Lippincott-Schwartz, and Harald F. Hess, “Imaging intracellular fluorescent proteins at nanometer resolution,” *Science* **313**, 1642–1645 (2006).
- [7] William E. Moerner, “New directions in single-molecule imaging and analysis,” *Proceedings of the National Academy of Sciences* **104**, 12596–12602 (2007).
- [8] Sripad Ram, E. Sally Ward, and Raimund J. Ober, “Beyond Rayleigh’s criterion: A resolution measure with application to single-molecule microscopy,” *Proceedings of the National Academy of Sciences of the United States of America* **103**, 4457–4462 (2006).
- [9] Harry L. Van Trees, *Detection, Estimation, and Modulation Theory, Part I*. (John Wiley & Sons, New York, 2001).
- [10] Larry A. Wasserman, *All of Statistics* (Springer, New York, 2004).
- [11] Mankei Tsang, “Quantum limits to optical point-source localization,” *Optica* **2**, 646–653 (2015).
- [12] Carl W. Helstrom, *Quantum Detection and Estimation Theory* (Academic Press, New York, 1976).
- [13] Alexander S. Holevo, *Statistical Structure of Quantum Theory* (Springer-Verlag, Berlin, 2001).
- [14] Vittorio Giovannetti, Seth Lloyd, and Lorenzo Maccone, “Advances in quantum metrology,” *Nature Photon.* **5**, 222–229 (2011).
- [15] Akio Fujiwara, “Strong consistency and asymptotic efficiency for adaptive quantum estimation problems,” *Journal of Physics A: Mathematical and General* **39**, 12489 (2006).
- [16] Jean-François Morizur, Lachlan Nicholls, Pu Jian, Seiji Armstrong, Nicolas Treps, Boris Hage, Magnus Hsu, Warwick Bowen, Jiri Janousek, and Hans-A. Bachor, “Programmable unitary spatial mode manipulation,” *J. Opt. Soc. Am. A* **27**, 2524–2531 (2010).
- [17] Seiji Armstrong, Jean-Francois Morizur, Jiri Janousek, Boris Hage, Nicolas Treps, Ping Koy Lam, and Hans-A. Bachor, “Programmable multimode quantum networks,” *Nature Commun.* **3**, 1026 (2012).
- [18] D. J. Richardson, J. M. Fini, and L. E. Nelson, “Space-division multiplexing in optical fibres,” *Nature Photon.* **7**, 354–362 (2013).
- [19] Horace P. Yuen and Jeffrey H. Shapiro, “Optical communication with two-photon coherent states—Part I: Quantum-state propagation and quantum-noise,” *IEEE Transactions on Information Theory* **24**, 657–668 (1978).
- [20] Mikhail I. Kolobov, “The spatial behavior of nonclassical light,” *Rev. Mod. Phys.* **71**, 1539–1589 (1999).
- [21] Nicolas Treps, Nicolai Grosse, Warwick P. Bowen, Claude Fabre, Hans-A. Bachor, and Ping Koy Lam, “A quantum laser pointer,” *Science* **301**, 940–943 (2003).
- [22] Agedi N. Boto, Pieter Kok, Daniel S. Abrams, Samuel L. Braunstein, Colin P. Williams, and Jonathan P. Dowling, “Quantum interferometric optical lithography: Exploiting entanglement to beat the diffraction limit,” *Phys. Rev. Lett.* **85**, 2733–2736 (2000).
- [23] Mankei Tsang, “Relationship between resolution enhancement and multiphoton absorption rate in quantum lithography,” *Phys. Rev. A* **75**, 043813 (2007).
- [24] Mankei Tsang, “Quantum imaging beyond the diffraction limit by optical centroid measurements,” *Phys. Rev. Lett.* **102**, 253601 (2009).
- [25] Vittorio Giovannetti, Seth Lloyd, Lorenzo Maccone, and Jeffrey H. Shapiro, “Sub-Rayleigh-diffraction-bound quantum imaging,” *Phys. Rev. A* **79**, 013827 (2009).
- [26] Baris I. Erkmen and Jeffrey H. Shapiro, “Ghost imaging: from quantum to classical to computational,” *Adv. Opt. Photon.* **2**, 405–450 (2010).
- [27] Ranjith Nair and Brent J. Yen, “Optimal quantum states for image sensing in loss,” *Phys. Rev. Lett.* **107**, 193602 (2011).
- [28] Heedeuk Shin, Kam Wai Clifford Chan, Hye Jeong Chang, and Robert W. Boyd, “Quantum spatial super-resolution by optical centroid measurements,” *Phys. Rev. Lett.* **107**, 083603 (2011).
- [29] Lee A. Rozema, James D. Bateman, Dylan H. Mahler, Ryo Okamoto, Amir Feizpour, Alex Hayat, and Aephraim M. Steinberg, “Scalable spatial superresolution using entangled photons,” *Phys. Rev. Lett.* **112**, 223602 (2014).
- [30] Philip R. Hemmer and Todd Zapata, “The universal scaling laws that determine the achievable resolution in different schemes for super-resolution imaging,” *Journal of Optics* **14**, 083002 (2012).
- [31] Carlos A. Pérez-Delgado, Mark E. Pearce, and Pieter Kok, “Fundamental limits of classical and quantum imaging,” *Phys. Rev. Lett.* **109**, 123601 (2012).

- [32] Michael A. Taylor, Jiri Janousek, Vincent Daria, Joachim Knittel, Boris Hage, Hans-A. Bachor, and Warwick P. Bowen, “Biological measurement beyond the quantum limit,” *Nature Photonics* **7**, 229–233 (2013).
- [33] Osip Schwartz, Jonathan M. Levitt, Ron Tenne, Stella Itzhakov, Zvicka Deutsch, and Dan Oron, “Superresolution microscopy with quantum emitters,” *Nano Letters* **13**, 5832–5836 (2013).
- [34] Jin-Ming Cui, Fang-Wen Sun, Xiang-Dong Chen, Zhao-Jun Gong, and Guang-Can Guo, “Quantum statistical imaging of particles without restriction of the diffraction limit,” *Phys. Rev. Lett.* **110**, 153901 (2013).
- [35] D. Gatto Monticone, K. Katamadze, P. Traina, E. Moreva, J. Forneris, I. Ruo-Berchera, P. Olivero, I. P. Degiovanni, G. Brida, and M. Genovese, “Beating the abbe diffraction limit in confocal microscopy via nonclassical photon statistics,” *Phys. Rev. Lett.* **113**, 143602 (2014).
- [36] Carl W. Helstrom, “Resolution of point sources of light as analyzed by quantum detection theory,” *IEEE Transactions on Information Theory* **19**, 389–398 (1973).
- [37] Leonard Mandel and Emil Wolf, *Optical Coherence and Quantum Optics* (Cambridge University Press, Cambridge, 1995).
- [38] Joseph W. Goodman, *Statistical Optics* (Wiley, New York, 1985).
- [39] Mankei Tsang, “Quantum nonlocality in weak-thermal-light interferometry,” *Phys. Rev. Lett.* **107**, 270402 (2011).
- [40] Joseph W. Goodman, *Introduction to Fourier Optics* (McGraw-Hill, New York, 2004).
- [41] Howard M. Wiseman and Gerard J. Milburn, *Quantum Measurement and Control* (Cambridge University Press, Cambridge, 2010).
- [42] Matteo G. A. Paris, “Quantum estimation for quantum technology,” *International Journal of Quantum Information* **7**, 125–137 (2009).
- [43] Samuel L. Braunstein and Carlton M. Caves, “Statistical distance and the geometry of quantum states,” *Phys. Rev. Lett.* **72**, 3439–3443 (1994).
- [44] Amnon Yariv, *Quantum Electronics* (Wiley, New York, 1989).
- [45] Amnon Yariv and Pochi Yeh, *Photonics: Optical Electronics in Modern Communications* (Oxford University Press, New York, 2007).
- [46] W. V. Sorin, B. Y. Kim, and H. J. Shaw, “Highly selective evanescent modal filter for two-mode optical fibers,” *Opt. Lett.* **11**, 581–583 (1986).